remote sensing

MDPI

Article

Experimental Evaluation of Several Key Factors Affecting Root Biomass Estimation by 1500 MHz Ground-Penetrating Radar

John C. Bain [1,*], Frank P. Day [1] and John R. Butnor [2]

[1] Department of Biological Sciences, Old Dominion University, Norfolk, VA 23529, USA; fday@odu.edu
[2] Southern Research Station, USDA Forest Service, Burlington, VT 05405, USA; jbutnor@fs.fed.us
* Correspondence: johncbain@gmail.com; Tel.: +1-757-589-2288

Received: 3 November 2017; Accepted: 17 December 2017; Published: 20 December 2017

Abstract: Accurate quantification of coarse roots without disturbance represents a gap in our understanding of belowground ecology. Ground penetrating radar (GPR) has shown significant promise for coarse root detection and measurement, however root orientation relative to scanning transect direction, the difficulty identifying dead root mass, and the effects of root shadowing are all key factors affecting biomass estimation that require additional research. Specifically, many aspects of GPR applicability for coarse root measurement have not been tested with a full range of antenna frequencies. We tested the effects of multiple scanning directions, root crossover, and root versus soil moisture content in a sand-hill mixed oak community using a 1500 MHz antenna, which provides higher resolution than the oft used 900 MHz antenna. Combining four scanning directions produced a significant relationship between GPR signal reflectance and coarse root biomass ($R^2 = 0.75$) ($p < 0.01$) and reduced variability encountered when fewer scanning directions were used. Additionally, significantly fewer roots were correctly identified when their moisture content was allowed to equalize with the surrounding soil ($p < 0.01$), providing evidence to support assertions that GPR cannot reliably identify dead root mass. The 1500 MHz antenna was able to identify roots in close proximity of each other as well as roots shadowed beneath shallower roots, providing higher precision than a 900 MHz antenna. As expected, using a 1500 MHz antenna eliminates some of the deficiency in precision observed in studies that utilized lower frequency antennas.

Keywords: coarse roots; ground penetrating radar; root biomass; 1500 MHz antenna

1. Introduction

Traditional methods for measuring root biomass, root architecture, and myriad other root characteristics are difficult, labor-intensive, and destructive [1–4]. Soil opacity and the large physical extent of some root systems have prevented accurate quantification [5–7] and have left significant gaps in understanding of belowground processes. Many models currently employed for measuring a variety of root growth functions are built on vegetative characteristics, which are highly variable both between and within species due to developmental asynchrony, and varying environmental and community interactions [8]. Long-term, in situ monitoring of roots is hampered by observational disturbance resulting in root systems and root growth being poorly defined relative to other areas of plant ecology [3]. A major limiting factor in understanding belowground processes and their role in terrestrial carbon sequestration has been the use of destructive measurement techniques (i.e., in-growth cores, soil cores, and pits) that inherently prevent temporal assessments in long-term studies [5,6,9–11].

To address these limitations, a number of nondestructive methods have been developed for measuring coarse roots, including radioisotope and stable isotope labeling, sap flow approaches, as well as geophysical imaging techniques [12–16]. Nondestructive methods allow for long-term

observation of coarse roots with a minimum amount of disturbance and, when combined with small-scale destructive methods for validation and calibration, have shown great potential [17]. The use of GPR to non-destructively image root systems provides an approach to address these knowledge gaps [7,13,18–24]. GPR has shown significant promise in quantifying belowground coarse root biomass. Many studies have revealed high correlations between GPR radargrams and root biomass [7,20–28], as well as high correlations with root diameter [19,26,29,30].

GPR propagates electromagnetic (EM) waves (50–2600 MHz) into the ground where they reflect off subsurface objects, such as roots, and are returned back to the surface [18,31]. Higher frequency waves provide higher resolution of roots; however, they experience signal attenuation more easily and thus do not penetrate as deep as lower frequency waves. Wave reflections result from differences in dielectric permittivity between adjacent objects and the soil [8,32,33]. Key measurement parameters are the two-way travel time and amplitude of reflected energy. Any reflection caused by a change in the EM wave velocity due to a change in dielectric permittivity will be displayed as a hyperbola due to the conical nature of the EM beam with the apex of the hyperbola indicating the actual location of the buried object [17,33–35]. In addition to object location, size and orientation can also be estimated, as well as water content, as differences in water content within a heterogeneous medium are the primary drivers of varying dielectric constants between objects [22,23,36].

Thousands of measurements are acquired in a gridded pattern of transects within a fixed study area, which can be processed and rendered into either two-dimensional (2-D) cross-sectional images of the soil or a three-dimensional (3-D) tomogram of the study area [37–40]. Repetitive measurement of a study area opens up the potential for non-destructive temporal observation of roots, allowing for quantification of root growth over time [8,22].

Technological advances leading to the development of higher frequency antennas has played a key role in the increase of GPR applicability for root detection over the last decade [22]. These advances allow for the use of lower frequency antennas for large scale (km) surveys, while higher frequency antennas can be applied for small scale (cm) studies where higher precision is necessary [22]. There are still areas of GPR applicability for coarse root measurement that require additional exploration, particularly in matching antenna frequency to desired outcome. The 900 MHz and 1500 MHz antennas are the most commonly used antennas for coarse root detection; however, certain parameters of applicability have not been thoroughly explored with both frequencies. Specifically, this study explores scanning methodology and transect configuration using a 1500 MHz antenna for small scale biomass estimation, dead root recognition, and potential complications due to root shadowing.

1.1. Transect Configuration

A number of studies have shown promising results estimating root biomass using GPR [7,19–21,25–30,41–45]. GPR has been shown to routinely identify roots as small as 5 mm in diameter in field soils using a 1500 MHz antenna [19]. Thus, 1500 MHz is the frequency of choice in root biomass estimation studies. Lower frequency antennas are not as useful for this application. However, these studies have only utilized either single direction scanning transects [7,19–21,25–27,29,30,42,44,45] or perpendicular, two-direction scanning transects [28,41,43]. It has been shown that the angle at which the GPR antenna crosses over a root affects the amplitude of the reflected waveform, thus affecting the estimated size of the root [46–48]. Guo et al. [48] examined a three-direction method to correct for non-perpendicular root orientation relative to the GPR transects, but did not extrapolate their data to system level biomass estimation. No research has been conducted to determine if models built using four scan directions have a higher potential to reduce variability based on root orientation compared to models based on fewer transect directions. While not as necessary for large scale applications, where variability can be overcome by larger sample sizes, small scale sampling is more space limited and thus more affected by variability as a result of root orientation. Due to the potential to underestimate biomass as a result of oblique root orientation, we sought to determine the accuracy of multiple

scanning directions, from a single direction up to four directions, set at 45° intervals, for estimating coarse root biomass.

1.2. Detection of Dead Roots

There are a number of other methodological concerns surrounding the application of GPR to coarse root measurement. Butnor et al. [21] found that live coarse root biomass does not correlate as well with GPR indexes as the combination of live and dead coarse roots. Additionally, some have pointed out that estimating coarse root biomass through GPR can be problematic due to root water content [17], suggesting that low root water content has a similar negative effect, as does high soil moisture. Previous studies have also shown that roots with low water content may be represented with weaker hyperbolic reflections, resulting in an underestimation of coarse root biomass [26,30]. Roots that are no longer living will continue to store carbon, but should see their water content equalize with the surrounding soil, potentially making them difficult to identify with GPR. While these roots will not lead to increased growth, they are still valuable relative to carbon storage; however, if there is not a large enough difference between root and soil moisture content, the expectation is that GPR will not identify dead roots. In order to quantify this potential difficulty, we examined simulated dead root fragments that were allowed to equalize their water content with the surrounding soil.

1.3. Root Shadowing

Stokes et al. [49] and Hirano et al. [30] found that GPR cannot reliably differentiate crossover patterns of roots as well as individual roots with small spaces between them. Leaf litter has also been shown to decrease root reflections [50]. These studies utilized a 900 MHz GPR antenna, which can consistently identify roots greater than 2 cm diameter [21]. A 1500 MHz antenna provides greater resolution of roots and potentially eliminates some of the inaccuracy in quantifying roots that are located close together or crossed over. Under ideal conditions, a 1500 MHz antenna is usually limited to the top 50 cm of soil, however, most tree roots are located within the first 50 cm of soil, so this is not problematic for this specific application [13,21,51]. Due to the difficulty experienced by Stokes et al. [49] and Hirano et al. [30] in accurately differentiating crossed over roots in close proximity with a 900 MHz antenna, the potential effects of small roots being hidden below larger, shallow roots were explored using a 1500 MHz antenna.

2. Materials and Methods

2.1. Site Description

The study site was located in the Blackwater Ecological Preserve, which covers approximately 1.25 km^2 in Isle of Wight County, Virginia (36°49′31.6″N; 76°51′18.6″W). The Blackwater Ecological Preserve has been owned and managed by Old Dominion University (Norfolk, Virginia) since 1985 and is noted for hosting the northern most longleaf pine (*Pinus palustris* Mill.) population in North America. The Preserve is located on a remnant estuarine terrace, formed approximately 120,000 years ago as a result of raised sea levels during the Sangamon Interglacial period and is currently contained within the Blackwater River valley [52].

The majority of the Preserve is composed of sand flat and sand-hill mixed oak communities; however, a black gum swamp, alluvial flat, and a river bluff associated with the Blackwater River are also present. The soils are typical of the Coastal Plain of Southeastern Virginia, ranging from fine sands to sandy loam throughout much of the Preserve. The site is located within a 1500 m^2 area of sand-hill mixed oak community that is composed of somewhat excessively drained Alaga fine sand and has second growth forest as a result of logging about 60 years ago [52]. The stand is primarily composed of *Pinus taeda* L. (24%), *Quercus falcata* Michx. (17%), *Q. nigra* L. (10%), *Morella cerifera* Small (12%), *Liquidambar styraciflua* L. (9%) and *Ilex opaca* Soland. (8%). The sand-hill mixed oak community was selected because of a relatively low tree density providing ample space to work while

maintaining adequate root density, and ideal soil composition for manipulation of soil characteristics. The experiments conducted in this study were carried out in dry, sandy soils in order to minimize the influence of other soil factors when evaluating experimental factors.

2.2. Dielectric Constant Determination

The dielectric constant is a measurement of a substance's ability to insulate an electrical charge relative to the insulation in a vacuum. The dielectric constant of the soil is a key determinant for the propagation speed of the electromagnetic GPR waves through the soil and it is necessary to determine the dielectric constant (k) of the soil that is being scanned as this ensures accurate representation of depth without distortion. The dielectric constant is dependent on many factors; such as soil moisture, minerology, temperature and barometric pressure, and thus may vary substantially day-to-day in a heterogeneous soil, and will vary between different locations.

In order to calculate an accurate dielectric constant, four 90 cm long, 1 cm diameter aluminum rods were placed in parallel within an excavated pit at increasing depths of 10 cm, 20 cm, 30 cm, and 40 cm. Half of each rod was inserted into the side of the pit so that it was covered by undisturbed soil, leaving the other half covered by disturbed soil once the pit was backfilled with the excavated sand [42]. All root matter was separated from the soil with a sieve before the soil was used to backfill the pit. Two transects were established for dielectric calibration, one for the half of each rod that was covered by undisturbed soil, while the second was located above the half of each rod that was covered by disturbed soil. The first transect was used when the GPR was used to scan undisturbed areas and the second transect for all measurements that occurred in experimental plots that were excavated and backfilled.

As the dielectric constant can vary day to day, the appropriate transect was scanned with GPR at the beginning of each measurement day, depending on the experiments to be conducted. All field scanning for this study was conducted using a 1500 MHz antenna connected to a SIR-3000 GPR Control Unit (Geophysical Survey Systems Inc., Nashua, NH, USA). Once a clear scan of the dielectric transect was acquired, the location of the rods was marked and known depth was entered into the GPR unit. The GPR software automatically adjusted the dielectric constant so that it matched the adjusted depths of the rods. This new dielectric value was recorded and a confirmation scan was taken to ensure that the rods were observed at their correct depths. The dielectric value for a given day was used for all scans conducted that day, unless a large weather change occurred, i.e., midday showers. Using the dielectric pit as a guide, it was determined that a range of 10 nanoseconds, a boxcar finite impulse response filter, and three-point manual gain (−15, 15, 20) resulted in the best GPR representations of the buried rods and these settings were used for all measurements taken on site (Table 1).

Table 1. System settings for the radar unit with a 1500 MHz antenna and post-collection data processing parameters.

Application	Soil Water Cont. (%)	Soil Dielectric (Unitless)	Scan/m	Range (ns)	Collection Filters	Post-Collection Filters				Image Analysis
						Pos. Corr.	Back. Rem.	Mig.	Hilbert Trans.	Amplitude Threshold
Cores	8	2.42	400	10	FIR (boxcar), gain −15, 15, 20	√	√	√	√	70–240
Biomass Plots	7	2.02	400	10	FIR (boxcar), gain −15, 15, 20	√	√	√	√	70–215
Live vs. Dead Exp.	6	4.25	400	10	FIR (boxcar), gain −15, 15, 20	√	√	√	√	70–205
Root Shadow. Exp.	7	3.39	400	10	FIR (boxcar), gain −15, 15, 20	√	√	√	√	70–205

2.3. Root Biomass Estimation

In March 2013, 30 soil core locations (15 cm diameter to a depth of 60 cm) within the study area were selected. These core locations were used to develop a regression showing the relationship between high amplitude pixels identified with GPR and actual coarse root biomass, and thus were specifically chosen to represent the full spectrum of root density found within the study site. Prior to coring, each location was scanned using a 1500 MHz GPR antenna. A guide string was stretched across each core, bisecting the center point. As four direction scanning had not been previously utilized, a laminated core-scanning guide (Figure 1) was created to allow for repeatable data collection in four specific relative directions. The core-scanning guide was centered and placed over the core, using the guide string for orientation. Each core was then scanned in four relative directions: (1) 0° (2) 45° (3) 90° and (4) 135°, by rotating the scan guide around the center point, over the guide string (these directions will be referred to by numbers 1–4 hereafter). Eight parallel transects were taken for each direction at intervals of 2 cm, with 400 scans per meter along each transect. All scanning was conducted with the 1500 MHz antenna mounted to a hand cart equipped to measure travel distance, to ensure that measurements were taken at equal intervals. This required the study areas to be clear of aboveground vegetation and debris, and to be relatively flat. Initially there were 32 transects per core; however, it was later determined that the scanning could be halved without significant loss of accuracy. Each transect extended an additional 15 cm in each direction beyond the 15 cm diameter circle, representing the core area to be excavated, to eliminate edge effects.

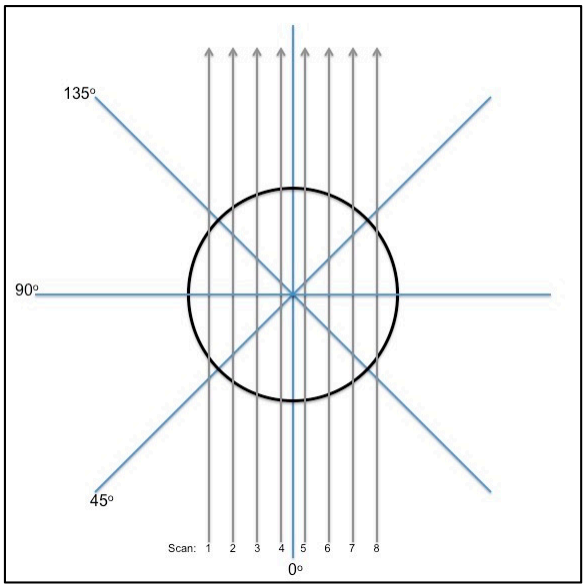

Figure 1. Ground penetrating radar (GPR) scan guide for 15 cm cores showing the four scan directions and the eight parallel transects with 2 cm spacing (32 scans per core).

After the scanning was completed for each core location, the cores were excavated to 60 cm depth and all roots greater than 5 mm were separated from the soil by dry sieving in the field. The remaining soil was then backfilled into the holes and the roots from each core were bagged separately and brought back to the lab for analysis. The roots were washed, oven dried for 48 h at 70 °C, and weighed to determine an oven-dried weight.

Processing of the radargrams was conducted using RADAN 7.0 (Geophysical Survey Systems Inc., Nashua, NH, USA) and SigmaScan Pro Image Analysis (Systat, San Jose, CA, USA) and followed the processing protocol described by Stover et al. [20] (Figure 2). Raw images were examined during collection to ensure appropriate data collection. These unprocessed radar grams could be interpreted to determine the presence of objects based on the presence of hyperbolic reflections; however, the size

and position of these objects cannot be accurately determined without further processing. The raw radargrams defaulted to y = 0 being the edge of the antenna; however, because of the presence of the hand cart, this point was not the soil surface. Once the raw image was brought into RADAN, the first processing step was a time zero filter, which removed the data collected between the antenna and the soil surface, and reset y = 0 to the soil surface. Secondly, a background removal filter was applied to reduce horizontal, non-target reflections, followed by a Kirchoff migration to migrate hyperbolic responses, thus correcting object position and collapsing diffractions [8]. Lastly a Hilbert transformation was used to eliminate the plus/minus nature of the electromagnetic pulse, rectifying the data into the positive domain, resulting in all positive value data, which could then be quantified along a continuum of weak-strong reflections [8]. These images were then converted to 8-bit grey scale using SigmaScan, with pixel intensities ranging from 0 (black) to 255 (white). Objects were identified as groups of pixels using a pixel intensity threshold. Variable soil conditions can result in the same object appearing larger or smaller via GPR, with more or fewer pixels within the limits of the threshold; thus, the appropriate values for the threshold were determined based on examining the dielectric scans collected the same day as the experimental data. Because the rods used in the dielectric pit were of known diameter, these images served as a guide as the threshold could be adjusted until the appropriate object size was observed. Once the threshold was applied, identified root objects were then quantified via pixel summation within groupings to determine the number of pixels representing roots. To provide the basis for biomass estimation, a linear regression was performed to quantify the relationship between observed root biomass from the soil cores and the number of pixels within the intensity threshold range from the GPR signals.

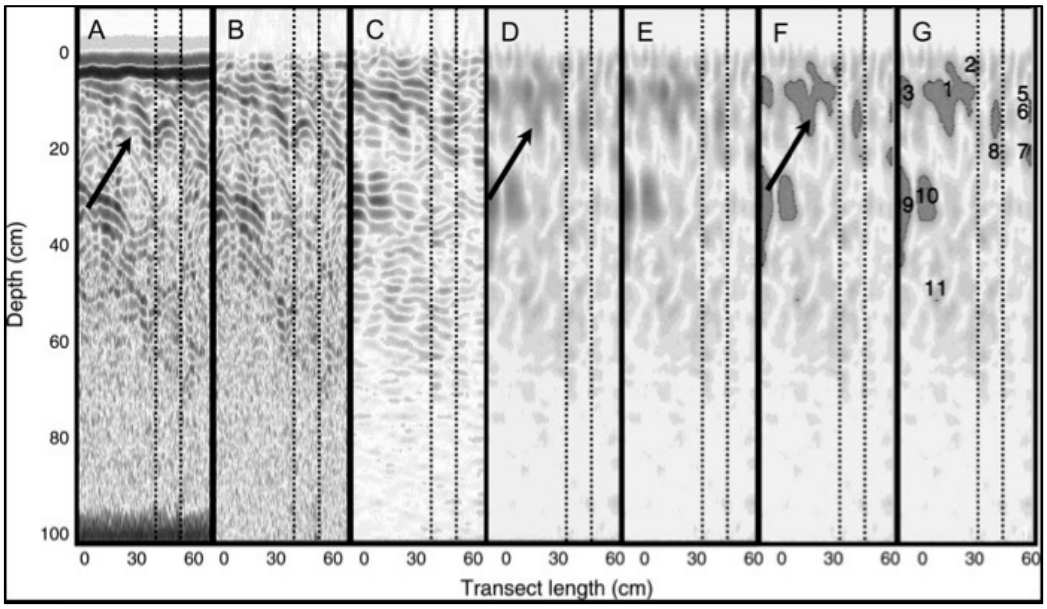

Figure 2. Radargram processing steps [20]. Arrows indicate a reflector (i.e., root). (**A**) Raw radargram; (**B**) Background removal to reduce noise; (**C**) Kirchoff migration to correct object position and hyperbolic geometry; (**D**) Hilbert transformation to enhance subtle objects and reduce false "echoes"; (**E**) Post-processed image converted to 8-bit grey scale; (**F**) Groupings determined based on pixel intensity; (**G**) Objects quantified via pixel summation within groupings.

In May 2013, 15 plots (0.25 m^2 area) were located to be used for experimental testing. Prior to excavation, each of these plots was scanned in the same four directions utilized to develop the regression equation in order to test the accuracy of the regression equation for biomass estimation. Each direction had five parallel transects set at intervals of 10 cm for the 0° and 90° directions and 14 cm for the 45° and 135° directions due to increased width of the plots when approached from

diagonal directions (Figure 3) and each transect had 400 scans per meter and extended 50 cm before the plot boundary and 15 cm beyond the plot boundary to eliminate edge effects.

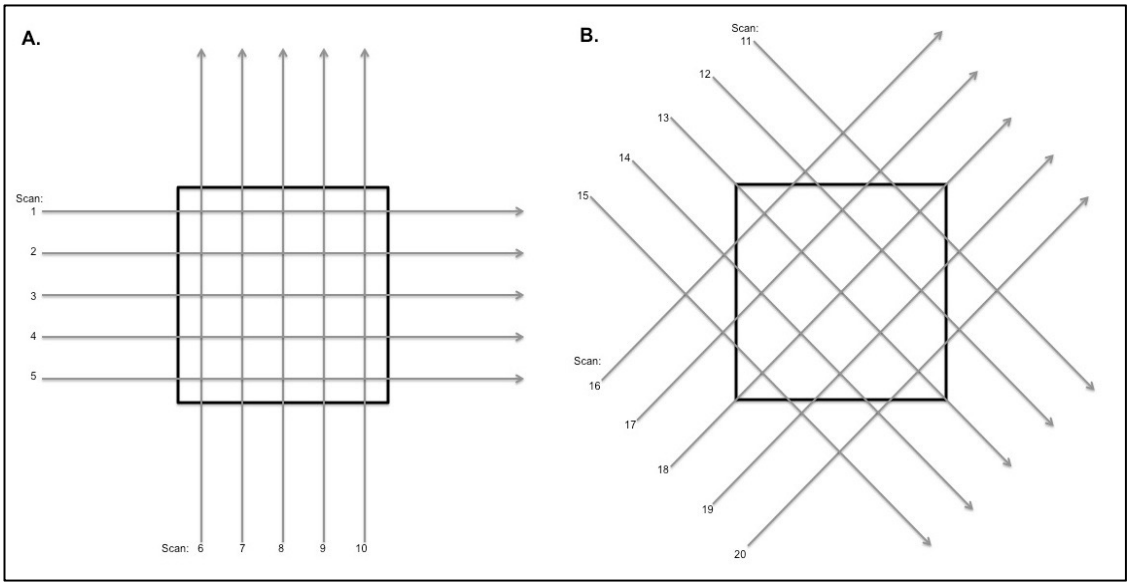

Figure 3. GPR scan guides for 0.25 m^2 plots showing the 5 parallel transects to be done in the (**A**) 0° and 90° directions [10 cm spacing] and (**B**) 45° and 135° directions [14 cm spacing].

Due to the greater size of the plots compared to cores and the limited space in which to operate around the plots, string scan guides were used rather than laminated sheet guides. Once scanning was completed, each plot was excavated to a depth of 60 cm and the roots were separated from the soil via sieving. The remaining soil was backfilled into the plots for later experiments. The roots were washed, oven dried for 48 h at 70 °C, and weighed to determine an oven-dried weight.

The GPR scans of the plots were processed using the protocol established during core sample analysis. Forty 15-cm core footprints (10 from each scanning direction) were selected in a grid pattern to represent "cores" within each plot. Using the regression equation developed from the cores, an average core footprint biomass within a given plot was determined by using the number of root image pixels identified within these core footprints. Since 14.14 15-cm cores equal 0.25 m^2, the average core footprint biomass of each plot was multiplied by 14.14 to determine an estimate of total biomass found within each 0.25 m^2 plot. A Wilcoxon Signed Ranks nonparametric test was used to determine if the estimated biomass was significantly different from the observed biomass in order to determine the effectiveness of GPR using different scan directions to accurately estimate coarse root biomass.

2.4. GPR Potential for Discrimination between Live and Dead Roots

This experiment utilized five of the previously excavated plots that had been refilled with the sieved soil from the biomass determinations. Four "live" roots and four "dead" roots were placed in each plot. "Live" roots were excavated on site and were wrapped with Parafilm to cover their cut ends to prevent moisture loss. To ensure minimal moisture loss, "live" roots were only used on the day they were excavated, however, testing showed that after an average initial root moisture content of 45%, these roots had 42% moisture content after one week buried on site. "Dead" roots were created from living roots that had been excavated from the site, oven dried for 24 h at 70 °C and reburied for a period of one week to ensure that their moisture content equalized with the local soil moisture, similar to the equalization that would occur when a non-disturbed section of root dies. The dead root fragments had an average root moisture content of 12% after one week in the soil. Although root moisture content was disrupted, decay consistent with dead roots was not included in the treatment.

The roots were placed 10 cm below the surface with the "live" and "dead" roots alternated throughout the plot. 10 cm depth was chosen as it was the typical depth of roots found on site as observed during previous excavation of cores and plots. Locations of both "live" and "dead" roots were documented for comparison to the GPR scans. All eight roots in each plot were oriented perpendicular to the scanning direction. Five parallel scans were taken at 10 cm intervals across each experimental plot for each of the five trials.

All scans were processed in RADAN and SigmaScan with the established protocol. Processed radargrams within RADAN were analyzed to determine the presence/absence of each root based on the presence/absence of pixels within the set pixel intensity threshold. Roots were determined to be present if objects with pixels within the determined pixel intensity range were identified within SigmaScan. A Mann-Whitney U test was used to determine the significance of roots seen versus unseen.

2.5. Possible Impacts of Root Shadowing on GPR Measurements

There were five treatment levels, with five trials of each treatment. The five treatment levels were: (1) no roots; (2) large roots at 3 cm depth with smaller roots at 13 cm depth; (3) large roots near surface removed; leaving smaller roots at 13 cm depth; (4) large roots at 10 cm with smaller roots below at 20 cm; and (5) no large roots at 10 cm leaving smaller roots below at 20 cm. In each treatment, four shadowing and four shadowed roots (obtained and prepared in the same manner as the "live" roots used in the previous experiment) were placed at the specified depth (one of each in each of the four quadrants of the plot), unless the treatment did not call for one or both of these groups.

All roots were approximately 20 cm in length, while large roots had a diameter of approximately 30 mm and small roots had a diameter of approximately 10 mm. All roots were oriented perpendicular to the scanning direction and five parallel scans were taken at 10 cm intervals across each experimental plot (15) for each treatment level.

All scans were processed in RADAN and SigmaScan with the established protocol. Processed radargrams within RADAN were analyzed to determine the presence/absence of each root based on the presence/absence of pixels within the set pixel intensity threshold. These radargrams were exported to SigmaScan in order to quantify the pixel counts of all roots present. Roots were determined to be present if objects with pixels within the determined pixel intensity range were identified within SigmaScan. The presence/absence of each root as well as the pixel counts of all roots present were used to determine the effectiveness of GPR to recognize roots under varying environmental conditions. For all experiments, a Mann-Whitney U test was used to determine the significance of roots seen versus unseen, and a Wilcoxon Signed Ranks test was used to quantify variability in observed pixel counts.

3. Results

3.1. Biomass Estimation

Linear regression of the data from the 15 cm cores using all four scan directions revealed a strong relationship between biomass and number of high-amplitude pixels: $y = 0.0346x + 5.9567$ ($R^2 = 0.7735$) ($p < 0.01$). Reducing the scanning effort by half (four scans per direction, a total of 16 scans per core), did not significantly change the coefficient of determination, as this relationship was still robust: $y = 0.0338x + 7.5286$ ($R^2 = 0.7536$) ($p < 0.01$) (Figure 4). Reducing the number of scanning directions from four yielded mixed results. Certain combinations of scanning directions utilizing either 1, 2, or 3 directions produced strong relationships, however each number of scan directions (1, 2, and 3) had at least one iteration resulting in noticeably lower regression strength (Table 2). Because of this potential for variability and the inability to predict which of the four directions should be used or avoided when estimating biomass of areas not excavated, it was determined that four directions offers the least risk of error. As such it was determined that four scans, in each of the four directions, was the

preferable method despite the need for increased scanning effort. Applying all four scan directions to the 0.25 m^2 plots and the grid pattern method of locating core footprints within the plot, the regression developed from the core data estimated 2525 ± 463 g/m^2 of coarse root biomass within the 0.25 m^2 plots, which was not significantly different from the observed biomass of 2637 g/m^2 ($p = 0.94$).

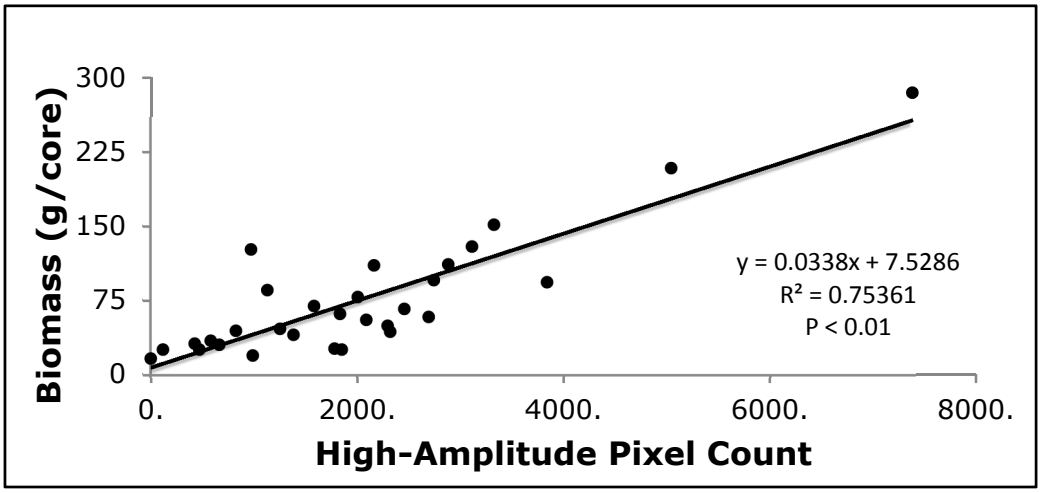

Figure 4. Relationship between total observed biomass obtained from 15 cm cores to a depth of 60 cm and GPR root reflectance as measured by high-amplitude pixels within the study site.

Table 2. Regression equations, coefficients of determination, biomass estimates developed from core scanning utilizing all possible different combinations of scanning directions, where 0°, 45°, 90°, and 135° are listed as directions 1, 2, 3, and 4, respectively, as well as the *p* values for the predicted versus observed biomass.

Scan Dir. Used	Regression Equation	R^2	Biomass Est. (g/m^2)	*p*
1	y = 0.0179x + 30.209	0.62419	2821	0.21
2	y = 0.0221x + 35.812	0.42631	3399	0.35
3	y = 0.0188x + 47.427	0.2789	3851	0.08
4	y = 0.0206x + 29.858	0.41167	2969	0.44
1 & 2	y = 0.025x + 21.532	0.67607	2771	0.52
1 & 3	y = 0.0314x + 12.092	0.78542	2637	0.69
1 & 4	y = 0.0205x + 29.963	0.41099	2967	0.44
2 & 3	y = 0.0264x + 32.071	0.45089	3454	0.18
2 & 4	y = 0.0311x + 13.18	0.6107	2677	0.96
3 & 4	y = 0.0282x + 23.23	0.49127	3066	0.73
1, 2, & 3	y = 0.032x + 13.519	0.73571	2752	0.79
1, 2, & 4	y = 0.029x + 12.286	0.71708	2496	0.36
1, 3, & 4	y = 0.032x + 8.8377	0.74547	2487	0.49
2, 3, & 4	y = 0.0328x + 15.297	0.59245	2902	0.66
1, 2, 3, & 4	y = 0.0338x + 7.5286	0.75361	2525	0.94

Actual Biomass: 2637 g/m^2.

3.2. GPR Potential for Discrimination between Live and Dead Roots

GPR was able to correctly identify all 20 "live" root segments used in the experiment, but was only able to identify 3 of the 20 "dead" roots that had acclimated their moisture content to the surrounding soil, representing a significant drop in detection efficiency ($p < 0.01$). GPR does not appear to reliably identify roots that do not maintain a different moisture content from that of their surrounding soil (Figure 5).

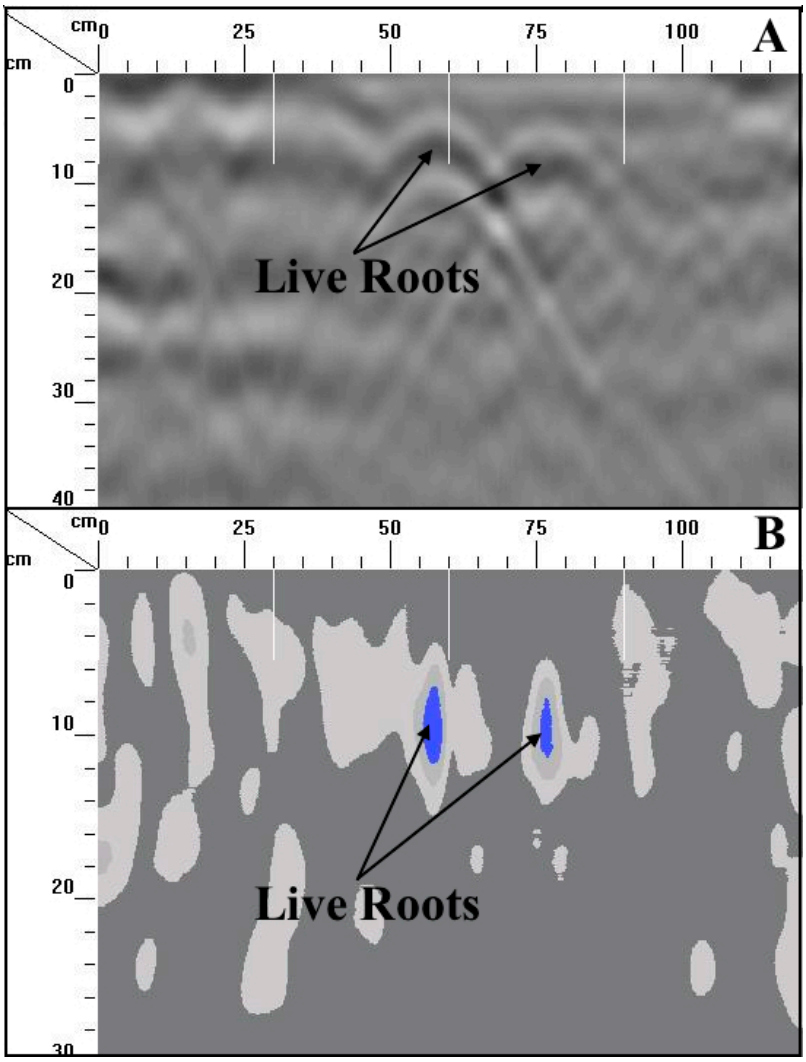

Figure 5. Radargrams (**A**) pre-processing and (**B**) post-processing images of a single transect scan during the "live" and "dead" root experiment showing only live roots were detected using GPR. Plots extend from 50 cm to 100 cm along the X-axis, and "live" roots were placed at approximately 10 cm intervals, such that "live" roots were found at 60 cm and 80 cm, while "dead" roots should have been seen at 70 cm and 90 cm.

3.3. Impacts of Root Shadowing on GPR Measurements

GPR was slightly less effective identifying small roots that were "shadowed" directly underneath larger roots, missing five out of 40 compared to only missing one small root when no large roots were present, but this was not a significant drop off in detection effectiveness ($p = 0.09$). Unshadowed roots were represented by an average of 3428 $\pm$ 188 pixels, while shadowed roots were represented by an average of 3215 $\pm$ 375 pixels. Additionally, there was not a significant difference between the number of pixels representing shadowed and unshadowed roots ($p = 0.51$). The one cause for concern appears in the variability of the pixel counts for shadowed roots, which displayed a standard error nearly double that of unshadowed roots, suggesting that while GPR is accurate for shadowed roots, it is not as precise when compared to unshadowed roots (Figures 6 and 7).

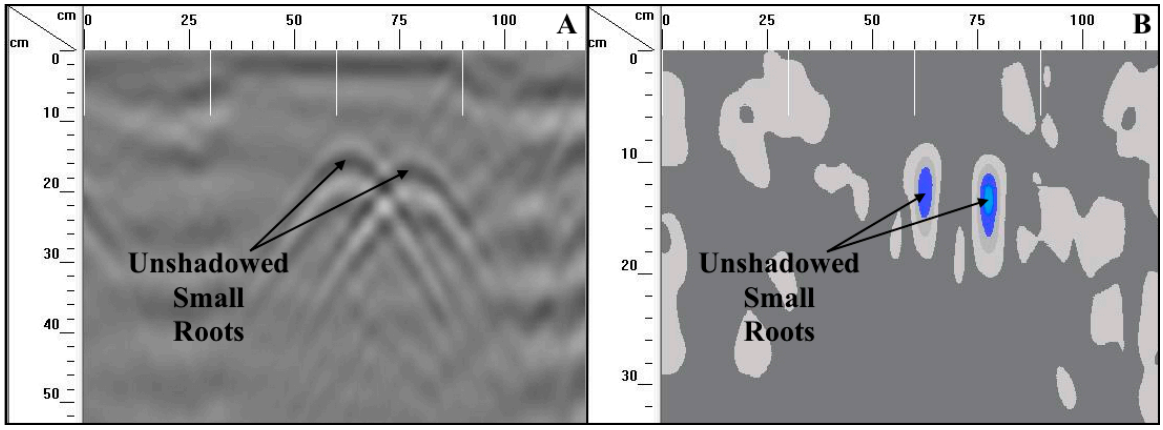

Figure 6. Radargrams (**A**) pre-processing and (**B**) post-processing images of two transects from the root shadowing experiment showing the GPR signature of 10 cm diameter roots when not shadowed by shallower roots above. Plots extend from 50 cm to 100 cm along the X-axis, and roots were placed at approximately 60 cm and 80 cm.

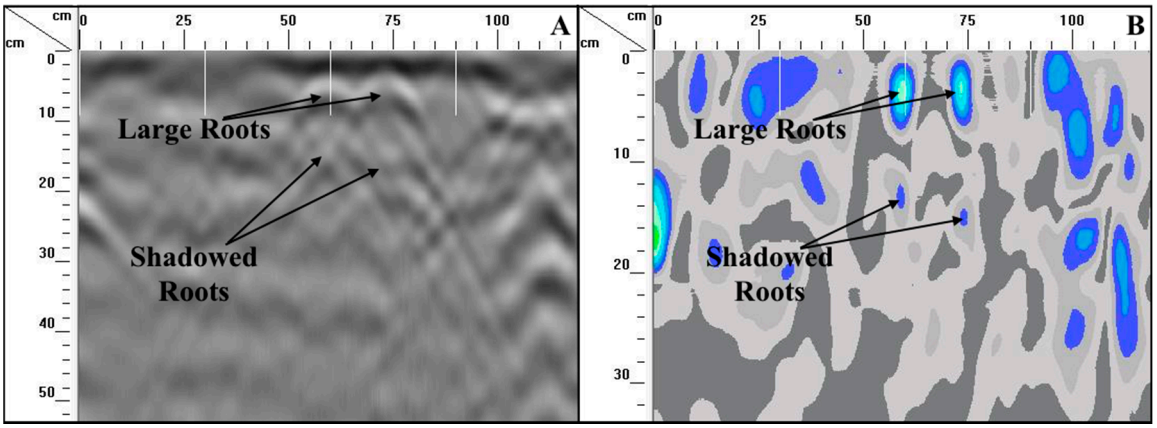

Figure 7. Radargrams (**A**) pre-processing and (**B**) post-processing images of two transects from the root shadowing experiment showing the GPR signature of 10 cm diameter roots when large roots are located 10 cm above and shadow the small roots. Plots extend from 50 cm to 100 cm along the X-axis, and roots were placed at approximately 60 cm and 80 cm.

4. Discussion

4.1. Impact of Scan Directions on Biomass Estimation

Strong regressions were obtained using total root biomass from sample cores to 60 cm depth, and using pixels within a threshold range for biomass estimation previously used by Stover et al. [20], Butnor et al. [2], Samuelson et al. [27,44,45], and Day et al. [43]. The number of transects in each direction was not paramount, but the inclusion of four scanning directions for each core and plot was important. There were multiple cores and plots in which scans from one direction showed significantly higher or lower estimated biomass than the other three, confirming the findings of Tanikawa et al. [46], Wu et al. [53], and Guo et al. [48] that root orientation significantly affects the accuracy of root detection and root diameter estimation. While two-direction scanning from the 2 & 4 directions produced the most accurate biomass estimate, the gross overestimate produced from using directions 2 & 3 demonstrated the potential for high variability in utilizing only two directions, which was resolved when all four directions were averaged together. It is important to note that the ability of GPR to estimate biomass within each pit varied with average variances from the observed biomass for

all scanning direction combinations ranging from 110–249 g/m^2, illustrating that multiple pits are necessary in order to counter potential small-scale variability in accuracy. For large scale efforts such as the forest stand level, variability can be constrained by a large sample size from scanning hundreds of meters, however this method is not feasible at small scales. Concentric circle scans can be applicable for examining roots around individual trees; however, this is only appropriate for certain applications.

4.2. GPR Potential for Discrimination between Live and Dead Roots

Multiple studies have shown that GPR has difficulty differentiating roots from other structures such as dead roots and PVC pipes [25,41]. The results of this study suggest that differences in root moisture content between live and dead roots have a significant effect on GPR effectiveness, despite the high level of precision of a 1500 MHz antenna in ideal soil conditions. The inability of GPR to accurately identify simulated "dead" coarse root fragments in this study appears to confirm previous work conducted with a 900 MHz antenna that root moisture content is an integral component of successful GPR applications [26,30]. Water has a high dielectric permittivity (80.1 at 20 °C) resulting in high levels of GPR signal attenuation. This can prevent the use of GPR in certain high moisture situations, but suggests that in low moisture situations, small changes in moisture levels should be easily detectable. Dannoura et al. [26] found that a sufficient gradient must exist between root moisture content and soil moisture level in order for roots to be detected. Dead root structures that are still a part of a larger living plant system may still be utilized for water conductance and could still be detectable; however, our results suggest that root structures that have been separated from the living organism or root systems that are a part of a larger dead organism would likely not be detectable. Since these structures are no longer being used for water conductance, their moisture content would equalize with that of the surrounding soil, making them invisible to GPR as the lack of a sufficient gradient of water content would mean no change in the speed of GPR wave propagation. This effect was confirmed by the ineffectiveness of GPR to identify simulated "dead" roots, which had been oven dried for 24 h at 70 °C and then reburied on site and left alone for one week so that they could equalize with the soil moisture levels.

As it will take significant lengths of time for dead root structures to decompose after their moisture content has become acclimated to the surrounding soil, the implication of this effect is the potential for underestimating total coarse root biomass for a given system. This is particularly pertinent for systems with slower decomposition rates and systems with higher organism turnover where unused root structures are more likely to be present, and could affect estimates of total belowground root biomass and total belowground carbon storage.

4.3. Impacts of Root Shadowing on GPR Measurements

Hirano et al. [30] showed that roots within 20 cm of each other could not be reliably distinguished from each other, while Stokes et al. [49] found that GPR has difficulty accurately representing roots that cross-over each other. As a result of this evidence, it was hypothesized that GPR would not be able to identify small diameter coarse roots that were placed 10 cm below and parallel to larger diameter coarse roots. While there were slightly fewer small roots accurately identified when a shadowing root was present, there was not a significant drop in the ability to identify roots that were both within 20 cm of and crossed-over by other larger roots. The most likely cause for this discrepancy from previous studies is twofold. First, six and 13 years had passed since the previous experiments were completed, during which time, significant technological and equipment advances have been made. Secondly, and more importantly, each of these studies utilized antennas of different frequencies. Stokes et al. [49] employed a 450 MHz antenna, resulting in the greatest detection depth (2.5 m) but also resulting in a significant loss of resolution. Higher frequencies result in higher resolution, but also higher signal attenuation and thus shallower maximum detection depths. Hirano et al. [30] were using a 900 MHz antenna, with slightly more resolution. The present study was conducted with a 1500 MHz antenna, which has been widely shown to be necessary for detection of 5 mm diameter roots [17]. With this

higher frequency and resolution, it should not be surprising that this study was able to identify and differentiate more roots than the previous two studies.

There is a concern that roots of the same size can appear smaller at deeper depths due to attenuation of the signal as it travels down through the soil. Cui et al. [54] modelled this effect and developed the following correction equation that can be used to account for this attenuation.

$$A(f, t) = C^{(-\alpha^* \times t)} \quad (1)$$

Here, $A(f, t)$ represents the amplitude of the two-way travel time (t); C is the true amplitude at a depth of 0 cm, when there is no signal attenuation; α^* is an attenuation factor based on the measurement frequency, and f is the measurement frequency. This does not appear to have been a significant factor in this experiment and was not deemed necessary, as the root fragments located at 20 cm depth were not significantly smaller than the same root fragments placed at 13 cm depth, actually resulting in a slightly higher mean number of pixels. This effect does still bear consideration, and the model would likely be necessary in more expansive future studies, particularly studies that place roots at depths greater than 20 cm.

The small number of shadowed roots that were not identified and the higher variability in predicted root size for shadowed roots suggest that even at this high frequency, GPR is slightly less effective in dealing with roots in close proximity to each other, but the differences in predicted size of the shadowed roots were not significantly different from estimates of size when no shadowing root was present. The balance between precision versus penetration depth shown in these studies points to the need to select the most appropriate antenna frequency before employing GPR for root quantification. Multiple antenna frequencies may be appropriate for root imaging, each with different strengths and weaknesses [16]. Choosing the most appropriate antenna or combination of antennas is crucial to a properly designed and executed GPR study.

5. Conclusions

Our results demonstrate that when using GPR for coarse root biomass estimation, one- and two-direction scanning does not produce biomass estimates that are significantly different from what was observed in the cores, but that utilizing multiple scanning directions can eliminate variability due to root orientation, and when possible, should be the preferred method. The data also support previous findings that a lack of significant difference between soil moisture and root moisture content significantly reduces the utility of GPR, suggesting that dead but not yet decomposed coarse roots are not represented in coarse root biomass estimates produced with GPR. GPR use for coarse root measurement is a young and growing area of belowground ecology, and is just one of many tools necessary to effectively measure root systems. These results should aid in the ongoing evolution of the use of GPR for coarse root measurements.

Acknowledgments: This material is based upon work supported by the Department of Energy under Award Number DE-SC0008099. We also want to thank the United States Forest Service Southern Research Station for additional funding. We thank Ben Webster, Jeff Rollins, Matt Stankavich, and James Chin for field assistance and root processing. We also appreciate Rachel Schroeder for her GPR expertise and advice during our experimental design.

Author Contributions: J.C.B., F.P.D., and J.R.B. designed the research. J.C.B. and F.P.D. performed experiments, conducted fieldwork, and collected data. J.C.B. analyzed the data. J.C.B., F.P.D., and J.R.B. wrote the manuscript.

Conflicts of Interest: The authors declare no conflict of interest.

References

1. Deans, J.D. Dynamics of coarse root production in a young plantation of Piceasitchensis. *Forestry* **1981**, *54*, 139–155. [CrossRef]

2. Oliveria, M.R.G.; van Noordwijk, M.; Gazeand, S.R.; Brouwer, G. Auger sampling, ingrowth cores and pinboard methods. In *Root Methods: A Handbook*; Smit, A.L., Bengough, A.G., van Noordwijk, M., Pellerin, S., van de Geijn, S.C., Eds.; Springer: Berlin, Germany, 2000; pp. 175–210.
3. Polomski, J.; Kuhn, N. Root research methods. In *Plant Roots: The Hidden Half*, 3rd ed.; Weisel, Y., Eshel, A., Kafkafi, U., Eds.; Marcel Dekker: New York, NY, USA, 2002; pp. 447–488.
4. Reubens, B.; Poesen, J.; Danjon, F.; Geudens, G.; Muys, B. The role of fine and coarse roots in shallow slope stability and soil erosion control with a focus on root system architecture: A review. *Trees* **2007**, *21*, 385–402. [CrossRef]
5. Fitter, A.H.; Stickland, T.R. Architectural analysis of plant root systems III: Studies on plants under field conditions. *New Phytol.* **1992**, *121*, 243–248. [CrossRef]
6. Nielsen, K.J.; Lynch, J.P.; Weiss, H.N. Fractal geometry of bean root systems: Correlations between spatial and fractal dimension. *Am. J. Bot.* **1997**, *84*, 26–33. [CrossRef] [PubMed]
7. Butnor, J.R.; Doolittle, J.A.; Johnsen, K.H.; Samuelson, L.; Stokes, T.; Kress, L. Utility of ground-penetrating radar as a root biomass survey tool in forest systems. *Soil Sci. Soc. Am. J.* **2003**, *67*, 1607–1615. [CrossRef]
8. Delgado, A.; Hays, D.B.; Bruton, R.K.; Ceballos, H.; Novo, A.; Boi, E.; Selvaraj, M.G. Ground penetrating radar: A case study for estimating root bulking rate in cassava (*Manihot esculenta* Crantz). *Plant Methods* **2017**, *13*, 65. [CrossRef] [PubMed]
9. Bledsoe, C.S.; Fahey, T.J.; Ruess, R.; Day, F.P. Measurement of static root parameters—Biomass, length, distribution. In *Standard Soil Methods for Long-Term Ecological Research*; Robertson, G.P., Bledsoe, C.S., Coleman, D.C., Sollins, P., Eds.; Oxford University Press: New York, NY, USA, 1999; pp. 413–436.
10. Fahey, T.J.; Bledsoe, C.S.; Day, F.P.; Ruess, R.; Smucker, A. Root production and demography. In *Standard Soil Methods for Long-Term Ecological Research*; Robertson, G.P., Bledsoe, C.S., Coleman, D.C., Sollins, P., Eds.; Oxford University Press: New York, NY, USA, 1999.
11. Norby, R.J.; Jackson, R.B. Root dynamics and global change: Seeking an ecosystem perspective. *New Phytol.* **2000**, *147*, 3–12. [CrossRef]
12. Berntson, G.M.; Farnsworth, E.J.; Bazzaz, F.A. Allocation, within and between organs, and the dynamics of root length changes in two birch species. *Oecologia* **1995**, *101*, 439–447. [CrossRef] [PubMed]
13. Hruska, J.; Cermak, J.; Sustek, S. Mapping tree root systems with ground-penetrating radar. *Tree Physiol.* **1999**, *19*, 125–130. [CrossRef] [PubMed]
14. Cermak, J.; Nadezhdina, N.; Meiresonne, L.; Ceulemans, R. Scots pine root distribution derived from radial sap flow patterns in stems of large leaning trees. *Plant Soil* **2008**, *305*, 61–75. [CrossRef]
15. Zenone, T.; Morelli, G.; Teobaldelli, M.; Fischanger, F.; Matteucci, M.; Sordini, M.; Armani, A.; Ferre, C.; Chiti, T.; Seufert, G. Preliminary use of ground-penetrating radar and electrical resistivity tomography to study tree roots in pine forests and poplar plantations. *Funct. Plant Biol.* **2008**, *35*, 1047–1058. [CrossRef]
16. Leucci, G. The use of three geophysical methods for 3D images of total root volume of soil in urban environments. *Explor. Geophys.* **2010**, *41*, 268–278. [CrossRef]
17. Guo, L.; Chen, J.; Cui, X.; Fan, B.; Lin, H. Application of ground penetrating radar for coarse root detection and quantification: A review. *Plant Soil* **2013**, *362*, 1–23. [CrossRef]
18. Wielopolski, L.; Hendey, G.; McGuigan, M. Imaging tree root systems in situ. *Proc. SPIE* **2000**, *4080*. [CrossRef]
19. Butnor, J.R.; Doolittle, J.A.; Kress, L.; Cohen, S.; Johnsen, K.H. Use of ground-penetrating radar to study tree roots in the southeastern United States. *Tree Physiol.* **2001**, *21*, 1269–1278. [CrossRef] [PubMed]
20. Stover, D.B.; Day, F.P.; Butnor, J.R.; Drake, B.G. Application of ground penetrating radar to quantify the effects of long-term CO_2 enrichment on coarse root biomass in a scrub-oak ecosystem at Kennedy Space Center. *Ecology* **2007**, *88*, 1328–1334. [CrossRef] [PubMed]
21. Butnor, J.R.; Stover, D.B.; Roth, B.; Johnsen, K.H.; Day, F.P.; McInnis, D. Using ground penetrating radar to estimate tree root mass: Comparing results from two Florida surveys. In *Handbook of Agricultural Geophysics*; Allred, B., Daniels, J.J., Ehsani, M.R., Eds.; CRC Press: London, UK, 2008; pp. 375–382.
22. Barone, P.M.; Ferrara, C.; Salvati, L. Tree root system imaging using Ground Penetrating Radar. *Ann. Silvic. Res.* **2017**, *41*, 67–70.
23. Ferrara, C.; Barone, P.M.; Pettinelli, E.; Salvati, L. Ground penetrating radar as a remote-sensing approach to investigate the root system architecture. *Appl. Ecol. Environ. Res.* **2014**, *12*, 695–702. [CrossRef]

24. Simms, J.E.; McKay, S.K.; McComas, R.W.; Fischenich, J.C. In situ root volume estimation using ground penetrating radar. *J. Environ. Eng. Geophys.* **2017**, *22*, 209–221. [CrossRef]
25. Butnor, J.R.; Roth, B.; Johnsen, K. *Feasibility of Using Ground-Penetrating Radar to Quantify Root Mass in Florida's Intensively Managed Pine Plantation*; Technical Report #38, Forest Biology Research Cooperative; University of Florida: Gainesville, FL, USA, 2005.
26. Dannoura, M.; Hirano, Y.; Igarashi, T.; Ishii, M.; Aono, K.; Yamase, K.; Kanazawa, Y. Detection of Cryptomeria japonica roots with ground penetrating radar. *Plant Biosyst.* **2008**, *142*, 375–380. [CrossRef]
27. Samuelson, L.J.; Butnor, J.R.; Maier, C.; Stokes, T.A.; Johnsen, K.; Kane, M. Growth and physiology of loblolly pine in response to long-term resource management: Defining growth potential in the southern United States. *Can. J. For. Res.* **2008**, *38*, 721–732. [CrossRef]
28. Borden, K.A.; Isaac, M.E.; Thevathasan, N.V.; Gordon, A.M.; Thomas, S.C. Estimating coarse root biomass with ground penetrating radar in a tree-based intercropping system. *Agrofor. Syst.* **2014**, *88*, 657–669. [CrossRef]
29. Barton, C.M.; Montagu, K.D. Detection of tree roots and determination of root diameters by ground penetrating radar under optimal conditions. *Tree Physiol.* **2004**, *24*, 1323–1331. [CrossRef] [PubMed]
30. Hirano, Y.; Dannoura, M.; Aono, K.; Igarashi, T.; Ishii, M.; Yamase, K.; Makita, N.; Kanazawa, Y. Limiting factors in the detection of tree roots using ground-penetrating radar. *Plant Soil* **2009**, *319*, 15–24. [CrossRef]
31. Daniels, D.J. *Ground Penetrating Radar*, 2nd ed.; Institution of Electrical Engineers: London, UK, 2004.
32. Al Hagrey, S.A. Geophysical imaging of root-zone, trunk, and moisture heterogeneity. *J. Exp. Bot.* **2007**, *58*, 839–854. [CrossRef] [PubMed]
33. Jol, H.M. *Ground Penetrating Radar Theory and Applications*, 1st ed.; Elsevier: Amsterdam, The Netherlands, 2008.
34. Annan, A.P.; Cosway, S.W. GPR frequency selection. In Proceedings of the 5th International Conference on Ground Penetrating Radar, Waterloo Center for Groundwater Research, Waterloo, ON, Canada, 12–16 June 1994; pp. 747–760.
35. Conyers, L.B. *Ground-Penetrating Radar for Archaeology*, 2nd ed.; Altamira Press: Walnut Creek, CA, USA, 2004.
36. Ferrara, C.; Barone, P.M.; Steelman, C.; Pettinelli, E.; Endres, A.L. Monitoring shallow soil water content under natural field conditions using the early-time GPR signal technique. *Vadose Zone J.* **2013**, *12*. [CrossRef]
37. Al-Nuaimy, W.; Huang, Y.; Nakhkash, M.; Fang, M.; Nguyen, V.; Eriksen, A. Automatic detection of buried utilities and solid objects with GPR using neural networks and pattern recognition. *J. Appl. Geophys.* **2000**, *43*, 157–165. [CrossRef]
38. Frigui, H.; Gader, P. Detection and discrimination of land mines in ground-penetrating radar based on edge histogram descriptors and a possibilistic-nearest neighbor classifier. *IEEE Trans. Fuzzy Syst.* **2009**, *17*, 185–199. [CrossRef]
39. Ho, K.; Carin, L.; Gader, P.D.; Wilson, J.N. An investigation of using the spectral characteristics from ground penetrating radar for landmine/clutter discrimination. *IEEE Trans. Geosci. Remote Sens.* **2008**, *46*, 1177–1191. [CrossRef]
40. Torrione, P.; Collins, L.M. Texture features for antitank landmine detection using ground penetrating radar. *IEEE Trans. Geosci. Remote Sens.* **2007**, *45*, 2374–2382. [CrossRef]
41. Cox, K.D.; Scherm, H.; Serman, N. Ground-penetrating radar to detect and quantify residual root fragments following peach orchard clearing. *HortTechnology* **2005**, *15*, 600–607.
42. Cui, X.H.; Chen, J.; Shen, J.S.; Cao, X.; Chen, X.H.; Zhu, X.L. Modeling tree root diameter and biomass by ground-penetrating radar. *Sci. China Earth Sci.* **2011**, *54*, 711–719. [CrossRef]
43. Day, F.P.; Schroeder, R.E.; Stover, D.B.; Brown, A.L.; Butnor, J.R.; Dilustro, J.; Hungate, B.A.; Dijkstra, P.; Duval, B.D.; Seller, T.J.; et al. The effects of 11 yr of CO_2 enrichment on roots in a Florida scrub-oakecosystem. *New Phytol.* **2013**, *200*, 778–787. [CrossRef] [PubMed]
44. Samuelson, L.J.; Stokes, T.A.; Butnor, J.R.; Johnsen, K.H.; Gonzalez-Benecke, C.A.; Anderson, P.; Jackson, J.; Ferrari, L.; Martin, T.A.; Cropper, W.P. Ecosystem carbon stocks in *Pinus palustris* forests. *Can. J. For. Res.* **2014**, *44*, 476–486. [CrossRef]
45. Samuelson, L.J.; Stokes, T.A.; Butnor, J.R.; Johnsen, K.H.; Gonzalez-Benecke, C.A.; Martin, T.A.; Cropper, W.P.; Anderson, P.H.; Ramirez, M.R.; Lewis, J.C. Ecosystem carbon density and allocation across a chronosequence of longleaf pine forests. *Ecol. Appl.* **2017**, *27*, 244–259. [CrossRef] [PubMed]

46. Tanikawa, T.; Hirano, Y.; Dannoura, M.; Yamase, K.; Aono, K.; Ishii, M.; Igarashi, T.; Ikeno, H.; Kanazawa, K. Root orientation can affect detection accuracy of ground-penetrating radar. *Plant Soil* **2013**, *373*, 317–327. [CrossRef]
47. Wu, Y.; Guo, L.; Li, W.; Cui, X.H.; Chen, J. Comment on: Root orientation can affect detection accuracy of ground-penetrating radar. *Plant Soil* **2014**, *380*, 441–444. [CrossRef]
48. Guo, L.; Wu, Y.; Chen, J.; Hirano, Y.; Tanikawa, T.; Li, W.; Cui, X.H. Calibrating the impact of root orientation on root quantification using ground-penetrating radar. *Plant Soil* **2015**, *395*, 289–305. [CrossRef]
49. Stokes, A.; Fourcaud, T.; Hruska, J.; Cermak, J.; Nadyezdhina, N.; Nadyezhdin, V.; Praus, L. An evaluation of different methods to investigate root system architecture of urban trees in situ: 1. Ground-penetrating radar. *J. Arboric.* **2002**, *28*, 2–10.
50. Tanikawa, T.; Ikeno, H.; Dannoura, M.; Yamase, K.; Aono, K.; Hirano, Y. Leaf litter thickness, but not plant species, can affect root detection by ground penetrating radar. *Plant Soil* **2016**, *408*, 271–283. [CrossRef]
51. Jim, C.Y. Protection of urban trees from trenching damage in compact city environments. *Cities* **2003**, *20*, 87–94. [CrossRef]
52. Frost, C.C.; Musselman, L.J. History and vegetation of the Blackwater Ecologic Preserve. *Castanea* **1987**, *52*, 15–46.
53. Wu, Y.; Guo, L.; Cui, X.H.; Chen, J.; Cao, X.; Lin, H. Ground-penetrating radar-based automatic reconstruction of three-dimensional coarse root system architecture. *Plant Soil* **2014**, *383*, 155–172. [CrossRef]
54. Cui, X.H.; Guo, L.; Chen, J.; Chen, X.H.; Zhu, X.L. Estimating tree-root biomass in different depths using ground-penetrating radar: Evidence from a controlled experiment. *IEEE Trans. Geosci. Remote Sens.* **2013**, *51*, 3410–3423. [CrossRef]